

# The structure and radiation spectra of illuminated accretion discs in AGN. I. Moderate illumination

A. Różańska<sup>1</sup>, A.-M. Dumont<sup>2</sup>, B. Czerny<sup>1</sup>, S. Collin<sup>2</sup>

<sup>1</sup>*N. Copernicus Astronomical Centre, Bartycka 18, 00-716 Warsaw, Poland*

<sup>2</sup>*Observatoire de Paris, Section de Meudon, Place Janssen, 92195 Meudon, France*

28 October 2018

## ABSTRACT

We present detailed computations of the vertical structure of an accretion disc illuminated by hard X-ray radiation with the code TITAN-NOAR suitable for Compton thick media. The energy generated via accretion is dissipated partially in the cold disc as well as in the X-ray source. We study the differences between the case where the X-ray source is in the form of a lamp post above the accretion disc and the case of a heavy corona. We consider radiative heating via Comptonization together with heating via photo-absorption on numerous heavy elements as carbon, oxygen, silicon, iron. The transfer in lines is precisely calculated. A better description of the heating/cooling through the inclusion of line transfer, a correct description of the temperature in the deeper layers, a correct description of the entire disc vertical structure, as well as the study of the possible coronal pressure effect, constitute an improvement in comparison to previous works.

We show that exact calculations of hydrostatic equilibrium and determination of the disc thickness has a crucial impact on the optical depth of the hot illuminated zone. We study the lamp post model for a low ( $\dot{m} = 0.03$ ) and high ( $\dot{m} = 0.3$ ) accretion rate. In both cases we assume a moderate illumination where the viscous flux equals the X-ray radiation flux. A highly ionized skin is created in the lamp post model, with the outgoing spectrum containing many emission lines and ionization edges in emission or absorption in the soft X-ray domain, as well as an iron line at  $\sim 7$  keV consisting of a blend of low ionization line from the deepest layers and hydrogen and helium like resonance line from the upper layers, and almost no absorption edge, contrary to the case of a slab of constant density. A full heavy corona completely suppresses the highly ionized zone on the top of the accretion disc and in such case the spectrum is featureless.

**Key words:** galaxies: active – accretion, accretion discs – black hole physics – galaxies:Seyfert, quasars – X-rays.

## 1 INTRODUCTION

Broad band spectra of active galactic nuclei (AGN) demonstrate the presence of both cold and hot plasma in the vicinity of a black hole. Furthermore, detailed analysis of X-ray spectra reveal that those two phases interact radiatively during their accretion on a central object (for recent review, see Collin et al. 2000, Reynolds 2000; see also Poutanen 1999 for the discussion of this problem in case of galactic black holes). However, the accretion pattern is still a subject of dispute and several detailed scenarios were proposed.

In most cases, a key element of the model is an accretion disc which extends, or does not, down to the marginally stable orbit. The disc surface is expected to be strongly irra-

diated by the X-ray emission containing a significant fraction of the observed bolometric luminosity of AGN.

At a given disc radius, two distinct situations are possible. The hot plasma may provide only a source of irradiating photons, being located well above the disc or at different radius (the 'lamp post' model), or it may be located at the considered radius, in hydrostatic equilibrium with the cold disc, additionally exerting a dynamical pressure on the cold disc surface (the 'heavy corona' model) and modifying strongly its ionization state (Różańska et al. 1999).

In both families of models the optically thick disc is illuminated by a hard X-ray flux. Those two cases, however, differ significantly with respect to the ionization state of the disc surface layers, as indicated by the study of Różańska et

al. (1999). The density at the surface of a disc, irradiated through some non-locally produced X-ray flux, is zero while the density of the disc with a corona is quite high due to the coronal pressure. This may lead to significant differences in the disc radiation spectra, both in the continuum and the properties of the iron  $K_{\alpha}$  line.

Careful approach to the modeling of the broad band disc spectra is essential in order to test both models, particularly in view of the first chance for true X-ray spectroscopy, coming with XMM and Chandra observations. Therefore, in this paper, we address the problem of the vertical structure and the spectrum of the radiation emitted by the illuminated disc in two extreme cases: with and without the dynamical effect of the corona.

For that purpose we consider the radiation transfer within the disc much more carefully than it was done by Różańska et al. (1999), applying to the surface layers the code TITAN developed by Dumont, Abrassart & Collin (2000 hereafter DAC00). This code also provides us with the continuum and line spectrum of the disc and is interfaced with a Monte Carlo code NOAR to take into account Compton diffusion properly, and particularly to compute the iron  $K_{\alpha}$  line profile and the high energy continuum.

This approach itself is an improvement in comparison to the earlier results on the radiation spectra of X-ray irradiated accretion discs, although it is still not free from important simplifications.

We first stress that all computations of disc structure and disc spectrum are (and will necessarily be) based on simplifying assumptions because the problem is too complicated to be solved exactly. And as it is not possible to make a 'uniform' improvement - it is worth to improve one aspect of the model at the expense of another one. But different approximations leading to different predictions, it is necessary to perform a detailed comparison of the results, and this is not possible unless exactly the same model is used in the computation. For instance Ballantyne et al. (2001) and Nayakshin et al. (2000) have computed the spectrum of an irradiated disc in hydrostatic equilibrium using codes similar to ours. In the most simple case (an irradiated slab with a constant density), with exactly the same parameters, the reflected spectrum predicted by the three codes shows important differences in the detailed spectral features as well as in the overall shape of the continuum (cf. Pequignot et al. 2001). Thus in order to judge the reliability of the results and to compare them to the observations it is absolutely necessary that all authors be very clear on the approximations made in their computations, so that everyone could be aware of them. This is what we try to do in the present paper.

As improvements with respect to other methods, we have chosen here mainly to favor the radiative transfer treatment (other codes use the escape probability approximation, especially for the lines), and to include a correct (but obviously model-dependent) description of the vertical structure of the viscous disc underlying the irradiated layers (other codes use rough estimates from vertically averaged models). These improvements are made at the expense of the atomic data. However though our computations include less atomic transitions than XSTAR (used by Nayakshin et al. 2000), they include more ions and transitions than Ballantyne et al. 2001.

In our approach the viscosity in the disc is proportional to the total (gas + radiation) pressure. Close to the surface we compute the radiative transfer of continuum and lines using two-stream approximation with non-LTE treatment and with heavy elements abundances as described in DAC00. Deeper inside the disc the diffusive radiative transport is assumed. Due to better heating/cooling description we are able to calculate regions with temperatures below  $\sim 10^5$ , well matching with the disc interior, i.e. full profiles of the disc from the surface to the equatorial plane.

We compute the emergent spectrum from the UV to the hard X-ray range, including features like the iron  $K_{\alpha}$  line.

This paper is restricted to a moderate illumination (the lamp post and the heavy corona models), with low and high accretion rate, while the following paper will be devoted to the high illumination case (the flares).

In section 2 we present the assumptions and numerical method of computation. The results are presented in section 3. The final sections are devoted to discussion and conclusions.

## 2 METHOD

### 2.1 Generalities

We consider the vertical structure of an illuminated accretion disc and the emitted spectra in two cases. In the first case hard X-ray emission is produced in an active region located above an accretion disc (the lamp post model), and in the second case X-rays come from a hot corona (the heavy corona model). The spectral distribution of X-rays is a free parameter of our model and in both cases it is assumed to be the same. The only difference is that corona is heavy and exerts a considerable pressure on the disc surface thus modifying its properties.

In the case of lamp post model the surface boundary conditions are the same as for a standard accretion disc, i.e. the density (and gas pressure) approaches zero at the surface.

In the case of corona above an accretion disc the electron temperature of the hot plasma is chosen arbitrarily, in agreement with observations. We do not consider any particular coronal model in this paper. The optical depth and the gas pressure of the corona are determined according to the spectral distribution and the electron temperature from the relation that the flux emitted by the corona  $F_X$  is produced via Compton cooling of hot electrons by the soft flux  $F_{soft}$  outgoing from the accretion disc. The non-zero value of the coronal gas pressure implies surface condition on the disc atmosphere.

The disc structure in both cases is calculated in the same way, and the presence or absence of the heavy corona influences the disc only through the surface boundary conditions. These computations require an assumption about the viscous energy generation within a disc. We adopt a standard  $\alpha$  viscosity model where the viscous stress is proportional to the total pressure.

The results depend on the mass of the central black hole,  $M$ , the distance from the center,  $r$ , the total flux generated by accretion,  $F_{gen}$  (or total accretion rate  $\dot{m}$ ), the fraction of energy generated in the X-ray source,  $f = F_X/F_{gen}$ ,

and its spectral shape, and finally on the viscosity parameter  $\alpha$ . Since we do not specify any coronal model, we assume in both cases that all the angular momentum is transported outwards by the disc, but only a fraction of the gravitational energy,  $1 - f$ , is dissipated in the disc. Therefore, the disc accretion rate is smaller than the total accretion rate which is the parameter of our model, because the flux dissipated in the disc,  $F_{disc}$ , is smaller than the total generated flux;  $F_{disc} = F_{gen} - F_X$ . Note that in the case of lamp post model  $f$  is not equal to  $L_X/L_{bol}$ .

The computations of the disc structure are done through iterations between the code solving the hydrostatic equilibrium equation and the code solving the radiation transfer, as described below.

## 2.2 The computation scheme

### 2.2.1 The beginning step

The first step of the computations is completed as described by Różańska et al. (1999 Section 2). The radiative transfer within the disc is treated in the diffusion approximation and the convective transport is also included. The viscous energy dissipation is given by the local  $\alpha$  viscosity description. The hydrostatic equilibrium completes the set of equations which fully determines the vertical temperature and the density profiles.

Thus, in the first step, we integrate the set of equations:

$$F = F_{rad} = -\frac{16\sigma T^3}{3\kappa\rho} \frac{dT}{dz}, \quad \nabla_{rad} \leq \nabla_{ad}, \quad (1)$$

$$F = F_{rad} + F_{conv}, \quad \nabla_{rad} > \nabla_{ad}, \quad (2)$$

$$\frac{dF}{dz} = \frac{3}{2}\alpha P\Omega_K(1-f) + \frac{1}{2}F_X\kappa\rho \exp(-\tau), \quad (3)$$

$$P = P_{gas} + P_{rad}, \quad (4)$$

$$\frac{1}{\rho} \frac{dP}{dz} = -\Omega_K^2 z, \quad (5)$$

where:  $F$ ,  $F_{rad}$ ,  $F_{conv}$ ,  $T$ ,  $\rho$ ,  $z$ ,  $P$ ,  $P_{gas}$ ,  $P_{rad}$ ,  $\Omega_K$ ,  $\sigma$  and  $\tau$  are respectively: the flux emitted by the disc, the flux carried by radiation, the flux carried by convection, the temperature, the density, the vertical coordinate, the total pressure, the gas pressure, the radiation pressure, the Keplerian angular velocity, the Stefan-Boltzman constant and the Rosseland mean optical depth.

The opacity  $\kappa$  (the Rosseland mean) as a function of density and temperature is taken from Alexander, Johnson & Rypma (1994) for  $\log T < 3.8$ , from Seaton et al. (1994) for  $\log T > 4.0$ , and it is interpolated between these two tables for intermediate values of the temperature.

For convection we adopt a simple description based on the mixing length theory used in stellar interiors.

For both models we assume that half of the flux  $F_X$  is directed toward the disc and this fraction is absorbed (the albedo equals zero in the first computational step). Therefore, in both cases we have the same boundary conditions on the flux and temperature at the surface. Using the Edington approximation we require:

$$F(H_d) = F_{soft} \equiv 0.5F_X + (1-f)F_{gen}, \quad (6)$$

$$\sigma T^4(H_d) = \frac{1}{2}\sigma T_{eff}^4 = \frac{1}{2}F_{soft}, \quad (7)$$

where  $H_d$  is half of the disc thickness actually determined by the boundary condition on the equatorial plane:

$$F(z = 0) = 0. \quad (8)$$

The third boundary condition is different for both models. In the lamp post model, the density at the disc surface is:

$$\rho(H_d) = 0. \quad (9)$$

In the heavy corona model this condition results from the value of the pressure at the basis of the corona and the requirement of pressure equilibrium between the disc and the corona:

$$\rho(H_d) = P_{gascor} \frac{\mu m_H}{k_B T(H_d)}. \quad (10)$$

Assuming the vertical component of the gravity to be vertically constant, the hydrostatic equilibrium of the corona leads to the gas pressure of corona:

$$P_{gascor} = \Omega_K^2 \frac{\tau_c}{\kappa_{es}} H_{cor}, \quad (11)$$

where the pressure scale-height of the isothermal corona is of the order of:

$$H_{cor} = \left( \frac{k_B T_{cor}}{\mu m_H \Omega_K^2} \right)^{1/2}, \quad (12)$$

where  $\kappa_{es}$  is the opacity for electron scattering,  $k_B$  - the Boltzman constant and  $m_H$  - the mass of hydrogen. We assume the value of the mean molecular weight  $\mu = 0.5$  appropriate for cosmic chemical composition. Note that the pressure scale height  $H_{cor}$  would be lower than in the case of variable gravity by a factor of  $\sqrt{2}$ . Those two previous equations are equivalent, but they show clearly the dependence of  $P_{gascor}$  and  $H_{cor}$  on the free parameter  $T_{cor}$ . The coronal plasma is taken to be a single temperature medium with  $T_{cor}$  equal to the electron temperature chosen arbitrarily at  $1 \times 10^9$  K (as suggested by observations of high energy cut off of X-ray spectrum). The optical thickness of the corona  $\tau_c$  is not a free parameter of our model, but it is determined by the energy equilibrium. Since the corona is cooled via seeds photons coming from the accretion disc, it should have a specific thickness to produce an X-ray power-law spectrum with the energy index chosen in our computations. We consider the case of an energy index  $\alpha_E = 0.9$ , and we compute the coronal optical depth using a simple Comptonization code (Czerny & Zbyszewska 1991) based on semi-analytical formulae and appropriate for optically thin media.

We take into account only gas pressure due to the corona in this first step. The radiation pressure due to illumination is included in the second step of iteration after solving radiative transfer.

We solve this two point boundary problem by a shooting method. The integration of equations presented in this section is performed by the second order Runge-Kutta scheme with adaptive stepsize, as in Pojmański (1986).

### 2.2.2 Radiative transfer in the surface layers

Knowing the vertical density profile we can solve the radiative transfer within the surface disc layers much more accurately using the code TITAN/NOAR of DAC00. TITAN is

based on Eddington two-stream approximation of the radiative transfer and works in plane-parallel geometry. Radiative transfer is computed both in lines and in continuum (i.e. lines are not treated with escape probability approach) so the code can be used for very inhomogeneous thick media, as in the present case.

Thermal equilibrium and ionization and statistical equilibrium of ions are computed in complete non-LTE for 10 elements and all corresponding ions. We consider following elemental abundances: H: 1, He: 0.085, C:  $3.3 \times 10^{-4}$ , N:  $9.1 \times 10^{-5}$ , O:  $6.6 \times 10^{-4}$ , Ne:  $8.3 \times 10^{-5}$ , Mg:  $2.6 \times 10^{-5}$ , Si:  $3.3 \times 10^{-5}$ , S:  $1.6 \times 10^{-5}$ , Fe:  $3.2 \times 10^{-5}$ , from Allen (1973). Comptonization is taken into account both in the thermal equilibrium and in the computation of the spectrum, through an iteration with the Monte Carlo code of Compton scattering, NOAR.

The radiative transfer equations for each frequency  $\nu$  can be written in the form:

$$\frac{1}{\sqrt{3}} \frac{dI_\nu^+}{dz} = -(k_\nu + \sigma_{es})I_\nu^+ + \frac{\sigma_{es}}{2}I_\nu^- + \eta_\nu \quad (13)$$

$$-\frac{1}{\sqrt{3}} \frac{dI_\nu^-}{dz} = -(k_\nu + \sigma_{es})I_\nu^- + \frac{\sigma_{es}}{2}I_\nu^+ + \eta_\nu \quad (14)$$

where  $z$  is the distance measured from the disc surface,  $k_\nu$  is the absorption coefficient in  $\text{cm}^{-1}$ ,  $\sigma_{es}$  is the electron scattering coefficient, and  $\eta_\nu$  is the emissivity.

The boundary conditions are imposed at the illuminated side of the disc surface and asymptotically in the disc interior.

The surface boundary condition is given by:

$$I_\nu^+(0) = \frac{\sqrt{3}}{2\pi} F_\nu^X \quad (15)$$

where  $F_\nu^X$  is the frequency dependent illuminated X-ray flux.

It is not necessary to continue with integrations down to the equatorial plane of the disc since non-LTE effects disappear completely when the optical depth is  $\sim 10$ , and where the diffusion approximation is satisfactory anyway.

Therefore we divide the disc arbitrarily into a surface layer of thickness  $d$  and the interior, like in the case of a stellar atmosphere problem. The disc interior is calculated in the diffusion approximation of radiative transfer, and the zone down to  $z = d$  is computed by TITAN. However, we have to impose a second boundary condition at  $z = d$  which will insure that the energy flux dissipated in the disc  $F_\nu^{disc}(d)$  will leave the interior:

$$I_\nu^-(d) = I_\nu^+(d) + \frac{\sqrt{3}}{2\pi} F_\nu^{disc}(d). \quad (16)$$

Since the disc computations provide us only with the frequency-integrated value of the flux  $F_{disc}$  dissipated in the disc and the value of the temperature at  $z = d$ , we determine the spectral shape of the flux using the non-grey diffusion approximation but neglecting the frequency dependence of the opacity coefficient

$$F_\nu^{disc}(d) = \frac{4\pi}{3} \frac{dB_\nu(T)}{d\tau} = F_{disc}(d) \frac{\pi B_\nu(T)}{4\sigma^4} \frac{x \exp(x)}{(\exp(x) - 1)}, \quad (17)$$

where  $x = h\nu/k_B T$ ,  $B_\nu(T)$  is the Planck function. This condition is equivalent to the condition used by NKK00 (Eq.14) in their illuminated disc model.

The code returns the temperature profile and the spectral shape of the emitted radiation. The results are not sensitive to the choice of  $d$  as long as  $\tau_{es}(d)$  is neither too small (smaller than 3) nor too large (larger than 30) since in the first case the radiative transfer of the incident X-ray flux is not described accurately, and in the second case the accumulated error of the computations made practically in LTE zone is too large. We arbitrarily choose  $\tau_{es}(d) \sim 6$ . In earlier works it was estimated that X-rays penetrate the disc atmosphere up to an optical depth approximately equal 3 (Sincell & Krolik 1997, NKK00)

### 2.2.3 Density profile from hydrostatic equilibrium

Having the new temperature profile of the surface layers from the code TITAN calculated for the density profile in the first step, we can calculate a new density profile from hydrostatic equilibrium. For that purpose we solve the entire disc structure basically as described in Section 2.2.1, but with few modifications. At a distance smaller than  $d$  from the disc surface we assume the temperature profile given by Section 2.2.2 and we do not solve the diffusive radiative transfer (Eqs. 1 - 3), while deeper within the disc we solve the full disc vertical structure equations including diffusive radiative transfer and heat generation. At this stage we also include the radiation pressure due to the incident radiation. Having the radiation field given by TITAN we determine this pressure component by:

$$\frac{dP_{rad}}{dz} = \frac{1}{c\sqrt{3}} \int k_\nu F_\nu d\nu, \quad (18)$$

where the radiation pressure on the surface is equal to  $F_X/c$ .

In the heavy corona model the value of the density at the disc surface changes in subsequent iterations due to the change of the surface temperature, since it is determined from the adopted value of the pressure at the basis of the corona. This differs from the case of the lamp post model where the surface density is zero through all iterations.

One full iteration is done after computing the temperature and density profiles. The new density profile is used to repeat radiative transfer computations as described in Section 2.2.2. We again divide the disc in a surface layer with optical thickness  $\tau_{es}(d) \sim 6$ , and the rest of the disc, where the diffusion approximation is adopted.

We repeat iterations between radiative transfer and density profile until the temperature profile does not change, and in section below we present the results.

### 2.2.4 Iron line

When the irradiated disc structure is determined we calculate in more detail the shape of the X-ray spectrum in order to determine more accurately the properties of the iron  $K_\alpha$  line. These computations are done by the Monte Carlo code NOAR described in detail by DAC00. This code describes the radiative transfer of line components coming from various iron ions, as determined by TITAN, and includes the line broadening due to Comptonization. It is used also after each TITAN run to provide the net (heating - cooling) Comptonization effect. We do not include here any kinematic broadening related to the systematic motion of emitting material thus providing an 'intrinsic spectrum' which

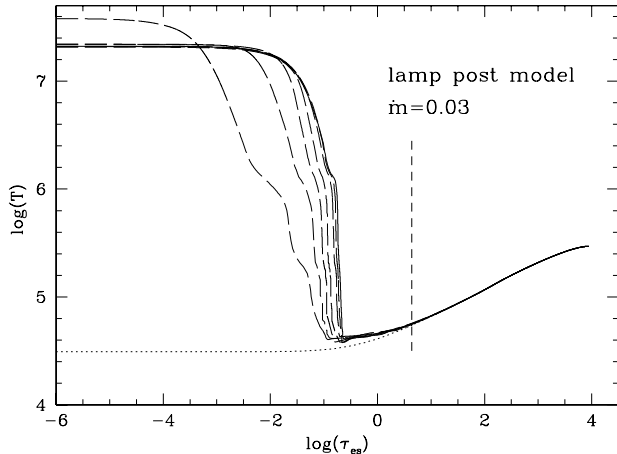


**Figure 1.** Temperature profile versus Thomson optical depth for the lamp post model. The initial profile is denoted by the dotted line, next iterations are presented as long dashed lines. The final profile is shown by the solid line. The vertical straight line marks the transition between the diffusion approximation and the exact solution.

later may be folded with arbitrary flow pattern like Keplerian disc motion, inflow or outflow.

### 3 NUMERICAL RESULTS

All results are presented for a single representative radius  $r = 10R_{Schw}$  (where  $R_{Schw} = 2GM/c^2$ ), for a mass of black hole  $M = 10^8 M_\odot$ , two accretion rates (in units of Eddington accretion rate with efficiency 1/12):  $\dot{m} = 0.03$  and  $\dot{m} = 0.3$ , a viscosity parameter  $\alpha = 0.1$ , and for  $f = 0.5$ . For these parameters, the total X-ray flux as well as locally dissipated flux are equal to  $6.96 \times 10^{13}$  erg s<sup>-1</sup> cm<sup>-2</sup>, with an incident X-ray radiation flux equal to half of this value.

The distribution of incident X-ray spectrum is a power-law with energy index  $\alpha_E = 0.9$ , extending from 2.8 eV up to 100 keV.

#### 3.1 Vertical structure of the disc without corona

We perform the coupled computation of the hydrostatic equilibrium and the radiative transfer for an irradiated accretion disc as described in Sect. 2.

We do not include conduction but the iterative method allows to pass effectively from the hot upper layers to the cold inner disc without serious instability problems. Contrary to the computations done by NKK00 we do not start calculation of radiative transfer from an already unstable temperature profile determined with the photoionization code. The successive iterations of the temperature profile for  $\dot{m} = 0.03$  are shown in Fig. 1 starting from the solution given by diffusion approximation (dotted line).

The temperature distribution displays an expected pattern; the hot upper layer reaches approximately the inverse Compton temperature (determined by the spectrum of the incident radiation and the radiation spectrum emitted by the disk and its atmosphere), then follows a rapid temperature drop due to an increase of the density and, consequently,

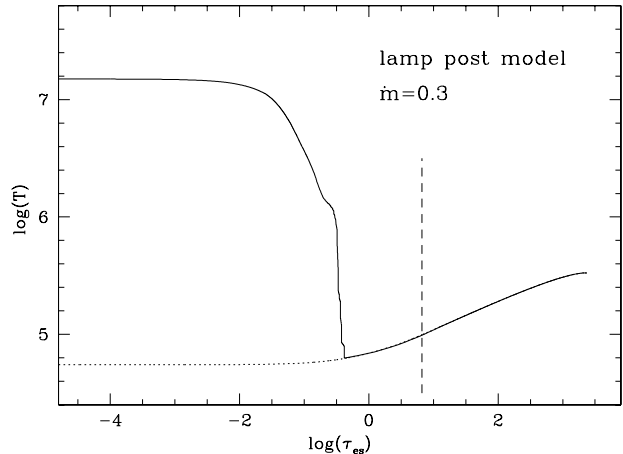


**Figure 2.** Temperature profile versus Thomson optical depth for the lamp post model. The initial profile is denoted by the dotted line and the final profile is shown by solid line. The vertical straight line marks the transition between the diffusion approximation and the exact solution.

an increase of the cooling efficiency of the gas. The deeper layers of the disc are not affected by the irradiation, so the better description of the radiative transfer than in the paper of Różańska et al. (1999) does not alter their results for the disc interior. After an initial decrease close to the surface, the temperature inside the disc is rising towards the equatorial plane, reaching  $T \sim 2.94 \times 10^5$  K. The solution converges satisfactorily after seven iterations. The number of iterations cannot be easily increased as the computations are time-consuming, taking about 3 days per iteration.

The temperature profile for the case of high accretion rate is presented in Fig. 2. The heated zone is thicker in this case than in the lower accretion rate solution.

In the final stage of iteration with radiative transfer we obtain an optical depth of the Compton heated skin  $\tau_{es}^{hot} \sim 0.03$  (defined by a decrease of the temperature by a factor 2 with respect to the surface temperature, in reference to the simple approach of Begelman, McKee and Shields 1983, the discussion of McKee and Begelman 1990 and Appendix A) for  $\dot{m} = 0.03$  and  $\tau_{es}^{hot} \sim 0.048$  for  $\dot{m} = 0.3$  (see Figs. 1 and 2). For  $\dot{m} = 0.03$  the height of the bare disc is  $H_d \sim 3.7 \times 10^{12}$  cm, and the height of the hot skin is  $H_{hot} \sim 5.1 \times 10^{12}$  cm. The transition layer is very thin, with  $H_{tran} = 6 \times 10^{11}$  cm. The same geometrical sizes in case of  $\dot{m} = 0.3$  are as follows:  $H_d \sim 2.3 \times 10^{13}$ ,  $H_{hot} \sim 1.44 \times 10^{12}$ , and  $H_{tran} = 1.1 \times 10^{11}$  cm. These values are much smaller than the disc radius ( $3 \times 10^{14}$  cm) which means that both the disc and the hot layer are geometrically thin.

Equation 12 gives analytically the scale-height of the Compton heated zone, when  $T_{cor}$  is replaced by the inverse Compton temperature  $T_{IC}$ . For the accretion rate  $\dot{m} = 0.03$  and  $T_{IC} = 2.1 \times 10^7$  K, as calculated from the spectral distribution of hard X-rays and the disc radiation, we can analytically derive the value of  $H_{hot} = 2.6 \times 10^{12}$  cm. We see that the actual thickness of the Compton skin is a factor of 2 larger when exact vertical calculations are done. The geometrical extension of the hot zone formally depends on the adopted value of the initial small (but non-zero) density

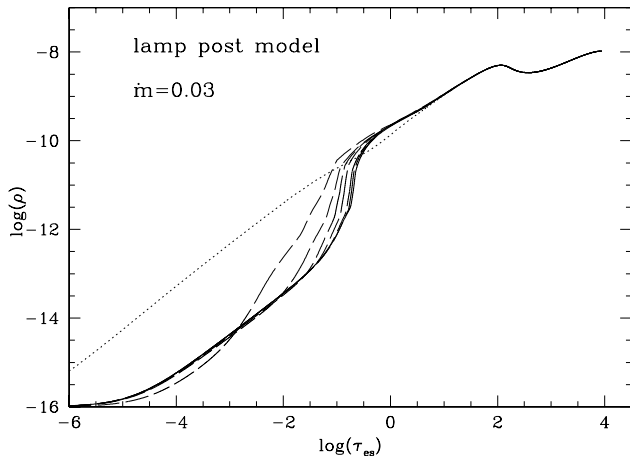


**Figure 3.** Density distribution versus Thomson optical depth for the lamp post model. The initial profile is denoted by dotted line, next iterations are presented as long dashed lines. Final profile is shown by the solid line.

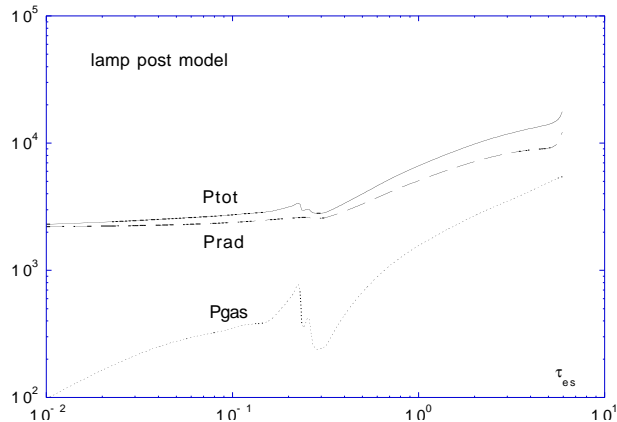


**Figure 4.** The pressure distribution versus Thomson optical depth in the surface layers for lamp post model after the last iteration for  $\dot{m} = 0.03$ .

at the surface but in practice this dependence is weak since the gravity in the disc increases outwards.

In Fig. 3 we show the density profile for  $\dot{m} = 0.03$ , again starting from the diffusion approximation. The density of the illuminated layer is lower than for the bare disc up to a Thomson optical depth  $\sim 0.1$ . Deeper in the disc, the density profile causes a density inversion due to convection, as shown in Różańska et al. (1999).

The final gas pressure and total pressure profiles for  $\dot{m} = 0.03$  are shown for surface zones in Fig. 4. Radiation pressure always dominates the gas pressure by at least two orders of magnitude.

The pressure profile resulting from diffusion approximation goes monotonically through the disc. Nevertheless in outer layers we see a 'wiggle' in the region of the temperature drop but the hydrostatic equilibrium and the radiative transfer are nevertheless computed with the required accuracy at each step. We argue here, that such 'wiggles' are due to thermally unstable regions, which are expected to appear in an atmosphere in hydrostatic equilibrium and illuminated by hard X-rays (RC96).

Since we start our computation from the thermally stable temperature profile of the non illuminated disc atmosphere, and since we perform an iteration between this profile and a single value density profile, we do not achieve a three value temperature profile (i.e. thermally unstable regions) after the radiative transfer computation. Note that iterating between temperature and density profiles is a usual way of treating any radiative transfer computations in hydrostatic equilibrium (see Hubeny 1990, Madej & Różańska 2000, NKK00). In thermally unstable regions, pressure is a monotonic function of optical depth (RC96), and therefore if we keep temperature as a single value function of  $\tau_{es}$  in our radiative transfer computations, the pressure inversion will appear in the thermally unstable region. We note, however, that the wiggle occupies only a small part of the irradiated layer and in particular it does not affect the overall shape of the emitted spectrum but it may have some impact on the detailed spectral features (cf. Sect. 4.1.3).

As a conclusion we stress that in any radiative transfer computation of disc atmospheres illuminated by hard X-rays, if the initial temperature profile does not display instabilities, the final pressure profile will display inversions. It may be the way to check that the cooling and heating are correctly computed, as the instabilities are due to discontinuities in the cooling rate through the illuminated atmosphere. Including the conduction flux into the scheme would solve the problem but it is technically difficult and no exact radiative transfer computations were performed with the conduction effect included up to now.

### 3.2 Outgoing spectrum in the lamp post model

#### 3.2.1 Overall spectral distribution

The reflected spectrum for  $\dot{m} = 0.03$ , obtained from the final iteration, is presented as a thick solid line in Fig. 5, which gives also the incident illuminating spectrum (power law line). The dashed line shows the observed spectrum, equal to the sum of the incident and the reflected spectra. Plotted spectra are usually degraded to a spectral resolution of  $R = 30$ , and no kinematic corrections are applied.

The reflected spectrum consists of a large optical/UV/soft X-ray component due to the disc emission as well as to thermalization of a significant fraction of the incident radiation. The X-ray part of the spectrum shows the characteristic spectral shape of reflection from partially ionized medium, with much more radiation in the soft X-ray band than in the case of a neutral medium (Lightman & White 1988), and in particular a lot of emission lines and ionization edges.

The reflected spectrum is very different from that of a constant density slab. It is actually not easy to compare precisely the two cases, as for hydrostatic equilibrium the ionization parameter has no meaning and it is also difficult to define an average density. To perform the comparison, we have used a slab of constant density equal to  $10^{12} \text{ cm}^{-3}$  with *exactly* the same irradiation as in the hydrostatic case: a power law spectrum with the same flux incident on the top of the layer, and a thermal spectrum incident on the bottom of the layer, with  $F_\nu^{disc}$  given by Eq. 17. This is comparable to the method used for instance by Ross et al (1993) and Życki et al (1994) to compute the disc spectrum, except

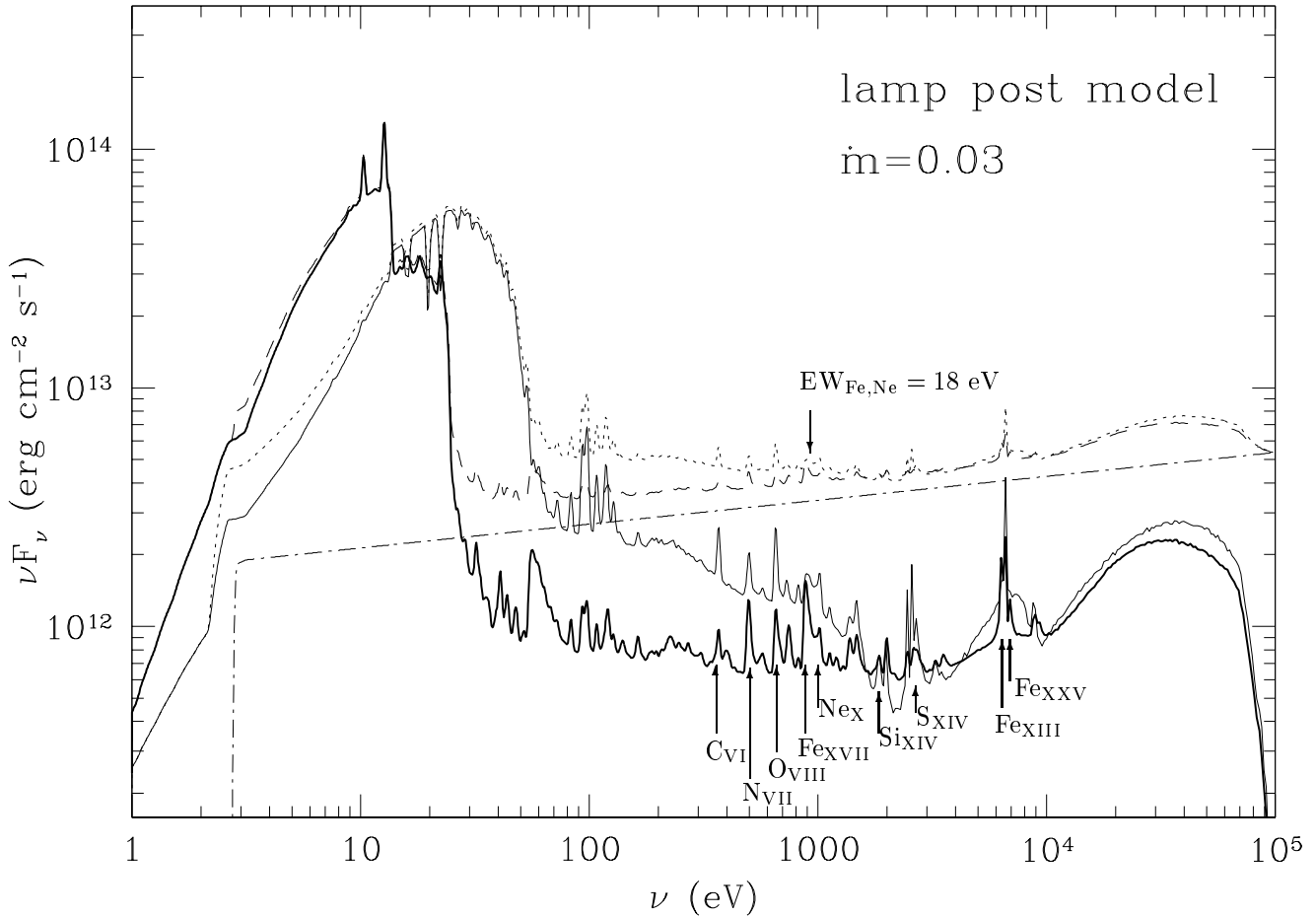


**Figure 5.** The reflected spectra of the irradiated disc for the lamp post model for hydrostatic equilibrium (thick solid line), and for constant density model (thin solid line). Final spectra are presented by dotted and dashed lines respectively. Power law line marks spectral distribution of incident radiation. Spectral resolution: 30.

that they had a larger density, representative of the mid-plane value, while we have a density more representative of the irradiated layers. The resulting reflected spectrum is displayed as a thin solid line on Fig. 5, in order to be compared with the lamp post reflected spectrum, and the corresponding observed spectrum is shown as a thin dotted line.

We see that the constant density case shows a larger thermal UV bump, very close to the underlying black body continuum, with only small traces of ionization edges in absorption, while the hydrostatic model exhibits a Lyman edge in absorption and a strong absorption above 20 eV, caused by the presence at  $0.1 \leq \tau_{es} \leq 1$  of several weakly ionized species: O II and O III, S II and S III, C III, Si II and Si III ions. As an illustration Figs. 6 a and b show the fractional abundances of the different iron ions as functions of the optical depth, respectively for the hydrostatic equilibrium and for the constant density case: in the latter case we see that only relatively highly ionized species are present in the deep layers, contrary to the hydrostatic case. In both cases highly ionized species are present at  $\tau_{es} \leq 0.1$ .

The low ionization state in the hydrostatic case is due to the high density of the deep layers. Since LTE is almost

reached, the ionization stage depends only on the density and the temperature profile. It is therefore *most important to solve the whole vertical structure of the disc to determine the abundances of these weakly ionized species and to get the correct spectral distribution in the far UV range*.

In the soft X-ray range the shape of the reflected spectra differs also in the two cases, as it is steeper for the constant density. This is due to the lack of thermal instability and consequently the smooth distribution of the temperature in the constant density case. On the contrary, the shape of the reflected spectrum in the hard X-ray range is almost the same in the two cases, as the Thomson thickness of the hot layer is relatively small ( $< 0.1$ ) so Compton reflection takes place in a cold medium. Also because of the small optical thickness of the hot skin, the outgoing spectrum is not modified by Comptonization in the UV and soft X-ray ranges. Finally, one should notice that in the soft and hard X-ray range the overall shape of the *observed* continuum is quite similar in the two cases, and it is only the (very different) detailed spectral features which could help to distinguish between them. In particular, the spectrum in the hydrostatic case exhibits strong ionization edges in emission in the soft X-ray range, but *no ionization edge of Iron* in absorption

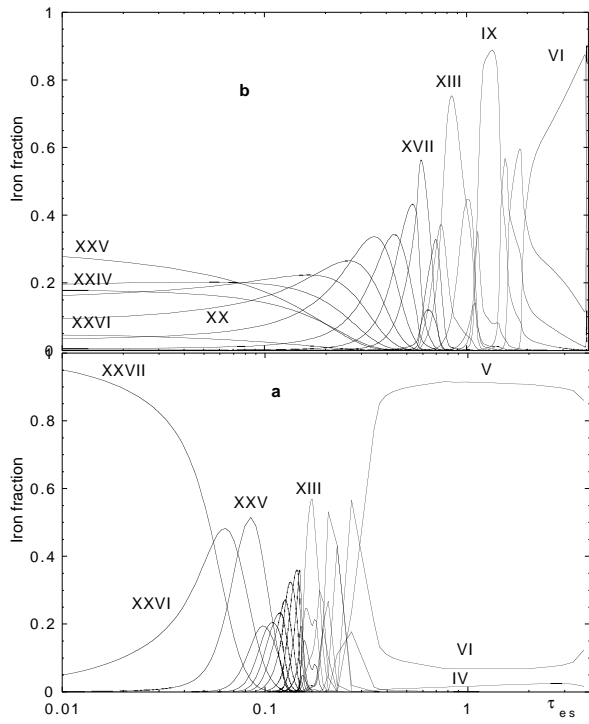


**Figure 6.** The fraction of iron ions in case of lamp post model versus Thomson optical depth in constant density case (upper panel) and hydrostatic equilibrium (lower panel). Accretion rate:  $\dot{m} = 0.03$ .

at  $\sim 10$  keV, contrary to the constant density case (see Figs. 5 and 9); one can see only a weak FeXXVI ionization edge in emission. Computations performed under assumption of constant pressure give results intermediate between the constant density and hydrostatic equilibrium solutions (Dumont et al. 2001).

The effect of the adopted value of the accretion rate can be seen comparing Figs. 5 and 7. The spectra are qualitatively similar, but they also show systematic differences matching the difference in the temperature profile.

The overall reflectivity in the X-ray band is higher for higher accretion rate, as it corresponds to somewhat higher ionization state of the gas. This is well seen in the plot of fractional abundances of iron (see Fig. 8). FeXXV is emitted predominantly from the optical depth of  $\sim 0.09$  for  $\dot{m} = 0.03$  but from the optical depth of  $\sim 0.18$  for  $\dot{m} = 0.3$  while FeV comes from  $\tau_{es} > 0.3$  and  $\tau_{es} > 0.7$ , correspondingly. There is systematically even more reflection in the soft X-ray band, making this case more similar to the constant density case than it was for lower accretion rate. Also for  $\dot{m} = 0.3$  there are copious soft X-ray lines from CNO elements and other species, although they are generally less intense than for  $\dot{m} = 0.03$  if measured with respect to the reflected component but have similar EW measured with respect to the total continuum. Higher average albedo leads to the reduced dominance of the optical/UV bump.

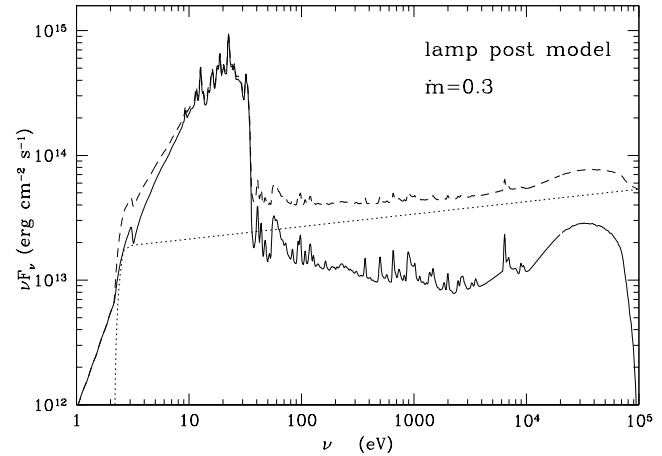


**Figure 7.** The reflected spectrum (continuous line) and final spectrum (dashed line) for the lamp post model in hydrostatic equilibrium for high accretion rate. Spectral resolution: 30.

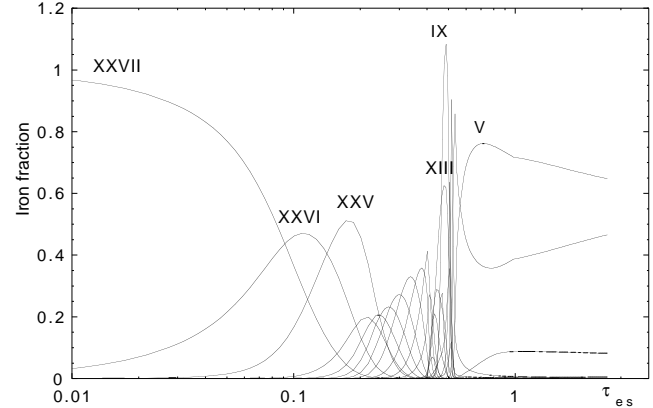


**Figure 8.** The fraction of iron ions in case of lamp post model versus Thomson optical depth in hydrostatic equilibrium. Accretion rate:  $\dot{m} = 0.3$ .

### 3.2.2 $K_\alpha$ line properties

The differences of ionization state in the two cases induce quite different Iron spectrum, as already stressed by NKK00 (who have performed a comparison using a constant irradiation flux and not a constant  $F_X/F_{visc}$  ratio like here). Figs. 9 and 10 display enlarged versions of the reflected spectra between 3 and 15 keV with relatively high spectral resolution. We see that in the hydrostatic case the spectrum is dominated by two components: the 6.4 keV component is due to several Iron  $K_\alpha$  lines of FeXIII and less ionized species (the most intense line being due to FeV), and the 6.7 keV component is the FeXXV recombination line blend with FeXXIV. For  $\dot{m} = 0.03$  the first one slightly dominates while for  $\dot{m} = 0.3$  the second one is stronger. The recombination line of FeXXVI is also present at 6.9 keV but is much weaker, as well as the  $K_\beta$  line at 7.1 keV. An emission edge due to FeXXV is seen at 8.8 keV. It is difficult to compute the equivalent width EW of each component separately, as they are blended together through Compton broadening. The whole line complex has

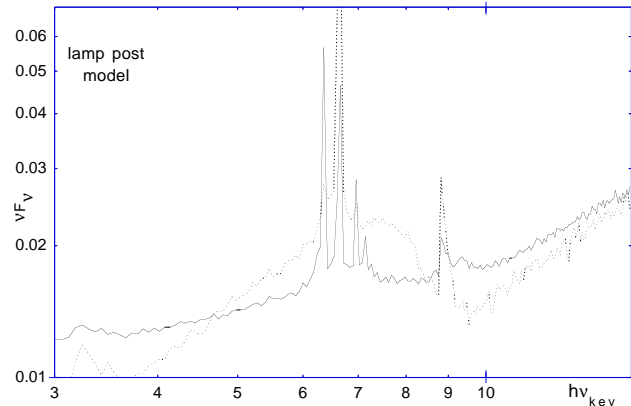


**Figure 9.** The close-up of the iron line region of the reflected spectrum (in arbitrary units) for lamp post geometry and constant density case (dotted line) and hydrostatic equilibrium (solid line). Spectral resolution  $R = 100$ . Accretion rate:  $\dot{m} = 0.03$ .

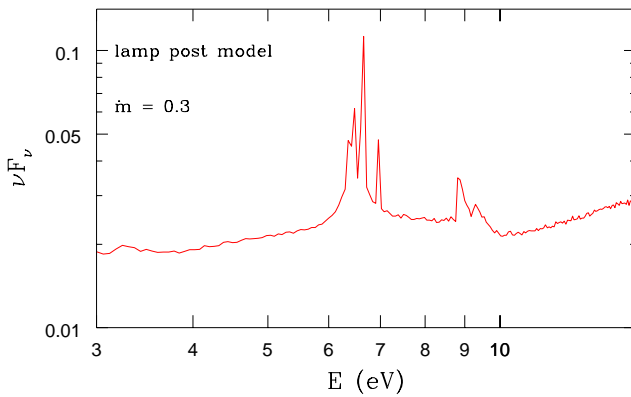


**Figure 10.** The close-up of the iron line region of the reflected spectrum (in arbitrary units) for lamp post geometry and hydrostatic equilibrium (solid line). Spectral resolution  $R = 100$ .

an EW of 550 eV with respect to the reflected continuum, corresponding to an EW of 90 eV with respect to the observed continuum in the case of the lower accretion rate. For high accretion rate, the corresponding numbers are 405 eV and 90 eV. Dividing roughly the whole line profile into the three lines, we obtain the values of the EW of the line components given with respect to reflected and total observed continuum, correspondingly (see Table 1).

These numbers are approximate: in particular the EW

**Table 1.** Iron  $K_{\alpha}$  line properties in the considered models\*.

component	$\dot{m} = 0.03$		$\dot{m} = 0.3$	
	$EW_{refl}$	$EW_{obs}$	$EW_{refl}$	$EW_{obs}$
cold Iron	240 eV	40 eV	145 eV	32 eV
FeXXIV+FeXXV	220 eV	37 eV	220 eV	49 eV
FeXXVI	80 eV	15 eV	40 eV	9 eV

\*  $F_x/F_d = 1$ ,  $\Gamma_{PL} = 2$ ,  $E_{max} = 100$  keV,  $M = 10^8 M_{\odot}$ ,  $r = 10R_{Schw}$

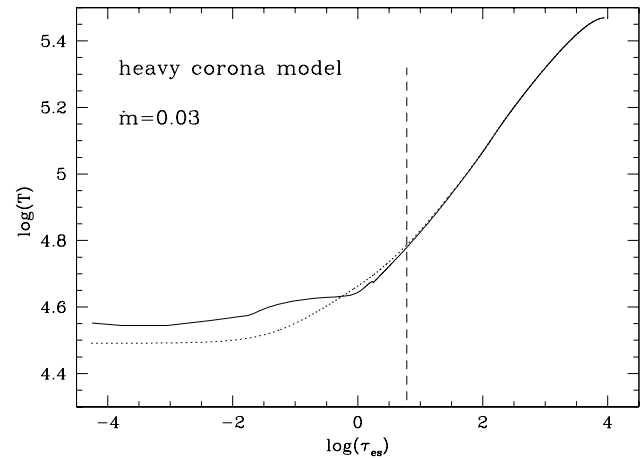


**Figure 11.** The temperature distribution for the heavy corona model. Initial profile is represented by dotted line, and final iteration by solid line.

of the FeXXVI line is overestimated, as it integrates a blue wing partly due to inverse Compton broadening of the other lines, and as a consequence the other lines are slightly underestimated.

In the constant density case the spectrum is dominated by the FeXXV line and by a corresponding intense ionization edge in emission. There is also a smooth but strong absorption above 8 keV due to the superposition of several ionization states.

### 3.3 The weight of the corona effect

#### 3.3.1 Vertical structure of the disc with coronal influence

In the case of the heavy corona we assume the electron temperature of the hot plasma to be equal  $1 \times 10^9$  K as expected from observations. This temperature and the assumed spectral distribution of X-rays imply an optical depth of corona  $\tau_{cor} = 0.355$  due to the role of Comptonization (Haardt & Maraschi 1991). Therefore, the coronal pressure, calculated from Eq. 11, is equal to 8200 in cgs units. All other parameters are the same as described in Sect. 3.1.

The dynamical pressure of the corona modifies the disc atmosphere, making the gas relatively cool and dense (Różańska et al. 1999).

The uppermost layers are heated up only by a factor of  $\sim 1.2$  (Fig. 11). The weight of the corona modifies the density of the surface layers and we show this effect in Fig. 12. The initial high value of the density decreases towards the disc interior forming the outer density inversion (see Różańska et al. 1999). Such inversion is reflected in the pressure variation versus Thomson optical depth (Fig. 12). Deeper gas density inversion is again connected with convection.

In the outer layers the gas pressure is comparable to the radiation pressure, but towards the equatorial plane the radiation pressure dominates even by two orders of magnitude.

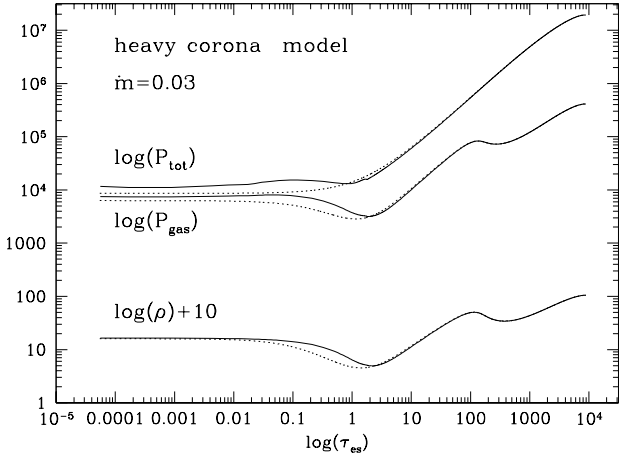


**Figure 12.** The distribution of density, gas pressure and total pressure for the heavy corona model. Initial profiles are presented by dotted line, and final iteration by solid line.

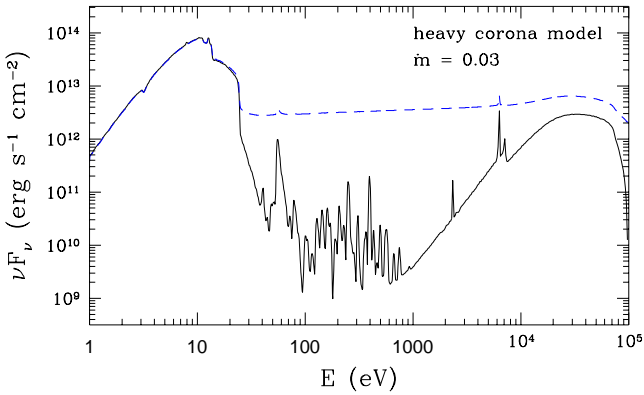


**Figure 13.** The spectrum of the irradiated disc with corona. Reflected spectrum - solid line, Comptonized reflected component - dashed line. Accretion rate:  $\dot{m} = 0.03$ .

### 3.3.2 Overall spectrum

The final spectrum as seen by the observer has to be calculated taking into account the direct presence of the corona.

In the case of a lamp post model we had to include, in agreement with equation 6, half of the incident X-ray radiation which goes directly to the observer (see final spectrum as a bold dotted line in Fig. 5). In the case of the corona model the radiation emerged from the disc is subsequently Comptonized by the hot coronal layer. To describe this effect we apply a simple code of Czerny & Zbyszewska (1991) based on semi-analytical formulae appropriate for optically thin Comptonized medium. This code does not include the effect of the anisotropy of Compton scattering. However, since in a bare disc model we also simplify the description of the fraction of the primary radiation going directly to an observer (we use the power law instead of Comptonized emission shape) such an approximation provides a better comparison of the two cases.

In Fig. 13 we present the reflected local spectrum by continuous line, while the dashed line represents reflected

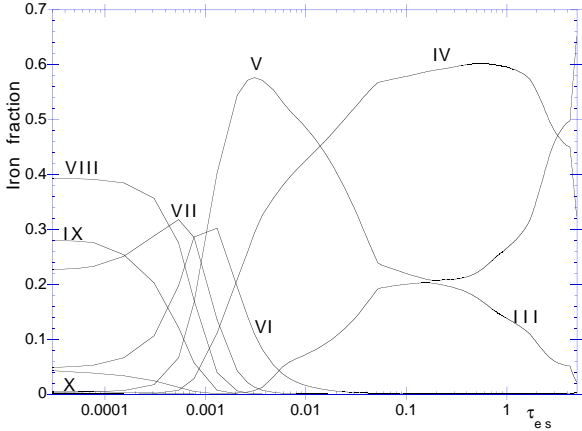


**Figure 14.** The fraction of abundances of iron ions for the heavy corona model, versus Thomson optical depth.

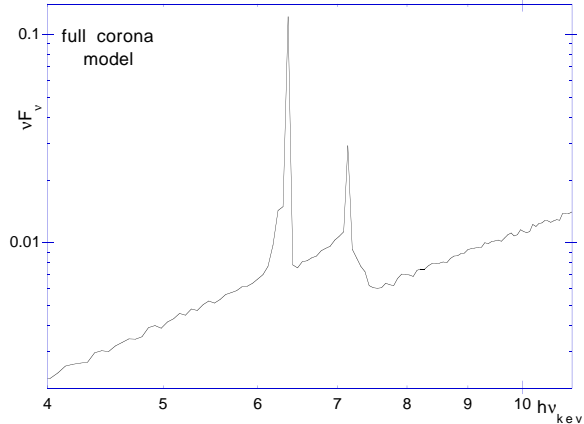


**Figure 15.** The close-up of the reflected spectrum (in arbitrary units) in the energy band of the iron line, for the heavy corona model. Spectral resolution  $R = 100$ . Accretion rate:  $\dot{m} = 0.03$ .

spectrum modified by its passing through the corona with temperature  $1 \times 10^9$  K and with  $\tau_{cor} = 0.355$ .

Such a corona, however, cannot cover the entire disc surface. According to our model, the sum of the energy emitted in X-rays and the energy emitted by disc cannot exceed the total energy generated due to accretion. Taking the assumed fraction of energy dissipated in the X-ray source  $f = 0.5$  and using Eq. 6 (albedo equal to zero) to describe the total outgoing soft flux, the Comptonized flux is given by:

$$F_X = A_C(0.5F_X + 0.5F_{gen}) = A_C(1.5F_X), \quad (19)$$

which gives the approximate constraint on the amplification factor:

$$A_C = 0.667. \quad (20)$$

Such Compton amplification in case of plane parallel coronal slab would give a very steep soft spectrum, inconsistent with the slope assumed in the computations. Our Comptonization code indicates that for the parameters  $\tau_{cor} = 0.355$  and  $T = 1 \times 10^9$  K (appropriate to reproduce the spectral index  $\alpha = 0.9$ ) the amplification is 3.9. Also

from simulations done by Abrassart & Czerny (2000, their Fig.3) one can see that in case of a disc black body spectral distribution with the temperature 50 eV the amplification factor never drops below 4 for a wide range of coronal temperatures. This is the main reason why a uniform non-patchy corona covering the entire disc is not a good model of Seyfert galaxies.

Since we model the entire spectrum at a single radius, we can circumvent this problem by breaking down the assumption of full, continuous corona and consider the case of a corona covering the disc only partially. We introduce a new parameter,  $f_{geom}$ , which decreases the probability of scattering of the soft photons in the corona due to its patchy structure. This parameter has to be included in Eq. 19 as:

$$F_X = A_C f_{geom} (0.5F_X + 0.5F_{gen}) = A_C f_{geom} (1.5F_X), \quad (21)$$

and implies the amplification factor to be:

$$A_C = \frac{0.667}{f_{geom}}. \quad (22)$$

Varying  $f_{geom}$  we can find the solution which preserves the required spectral slope, and the amount of coronal material which has to cover the cold disc to maintain energy balance between the hot and cold phases.

Fig. 13 shows that the spectrum reflected from the disc part covered by the corona and the observed spectrum from that radius is clearly a reflection from a basically neutral gas. No strong soft X-ray lines, characteristic of the lamp post geometry, are visible. Even at the disc surface the iron is only weakly ionized (Fig. 14). Only the 6.4 keV iron line is visible in the expanded picture of the 4-10 keV band, with relatively strong  $K_\beta$  line and considerable edge (Fig. 15).

However, the final spectrum of the object is not just a spectrum at the radius covered by the corona, but also the contribution from the uncovered part has to be included, in agreement with the required covering fraction. In our specific case with parameters: spectral slope  $\alpha = 0.9$  and fraction of energy dissipated in the corona equal 1/2,  $f_{geom}$  is very small,  $\sim 0.13$ , and the additional contribution ( $\sim 0.87$ ) from disc radii uncovered by the corona will dominate the total spectrum. In this case it would be impossible to distinguish between the lamp post and the patchy corona models.

However, in sources with a weaker Big Blue Bump (i.e. a small fraction of energy dissipated in the disc)  $f_{geom}$  is about 0.5 and the spectrum from a heavy corona model would approximately look like the spectrum in the lamp post geometry but with soft X-ray lines suppressed by a factor of order of 2. In sources with softer (steeper) X-ray spectra, slab amplification is significantly lower and the clumpiness of the corona is not needed. Therefore, in soft spectra sources, whenever the disc is covered by the corona, we would not expect any soft X-ray lines.

### 3.4 Comparison with observations

There are several interesting new observations of iron line done by satellites as BeppoSAX, XMM and CHANDRA. They usually report that iron line is rather narrow without relativistic broadening (Yaqoob, George, Nandra et al. 2001). Reeves et al. (2001) showed observations of the radio quiet quasar Markarian 205 where two components of iron line are present: a narrow neutral line at 6.4 keV and

a broadened line centered at 6.7 keV. They concluded that those observations are consistent with a disc origin only if the disc ionization is high enough to produce He-like iron, and if the narrow neutral component is produced elsewhere. But those conclusions were obtained by fitting the data with constant density models. Our model of illuminated disc in hydrostatic equilibrium shows that both components of iron line are present. The ionization state varies across the atmosphere and therefore we get a recombination iron line from uppermost layers and a fluorescence line from deeper zones. Also the EW of fluorescence line in our model ( $EW = 40$  eV for  $\dot{m} = 0.03$ ) is not in bad agreement with the observations (see Reeves et al. 2001 Table 1) where EW is 46 eV.

Another interesting observation, which could be fitted by our model, was reported by Comastri, Stirpe, Vignali et al. (2001). They observed the bright Narrow-Line Seyfert 1 galaxy Ark 564 and they reported a strong iron line from He-like iron line at  $\sim 6.76$  keV. The EW of the line estimated from an ionized reflection model is  $\sim 87$  eV. In our model with high accretion rate we obtain predominantly 6.7 keV component, with EW of  $\sim 90$  eV. However, we must notice that this source has much softer X-ray spectrum (photon index  $\Gamma \sim 2.5$ , Comastri et al. 2001, Turner et al. 2001).

Using our model, the emission lines from other elements such as oxygen, nitrogen and carbon can be determined. Branduardi-Raymont et al (2001) have observed the spectrum of MCG -6 -30 -15 in the soft X-ray range with XMM. They claimed that the very intense and broad features in this object cannot be attributed to a warm absorber, but are emission lines produced by an irradiated accretion disc and relativistically broadened. This result was not confirmed by the analysis of the CHANDRA data, as reported by Lee et al. (2001). Our model shows that irradiated accretion discs with moderate illumination *cannot* produce very strong emission lines. The results presented in this paper (Figs. 5 and 7) show that the most prominent line (doublet  $N_{\text{ex}} \text{Fe}_{\text{XVII}}$ ) has  $EW \sim 18$  eV (for both  $\dot{m} = 0.03$  and  $\dot{m} = 0.3$ ) in comparison to the emitted continuum.

## 4 DISCUSSION

### 4.1 Precision of the method, advantages and drawbacks

#### 4.1.1 Radiative transfer

In the present paper we do not recall the influence of the transfer treatment, which was discussed in DAC 2000 and in Dumont & Collin 2001. It was for instance shown that it is most important to take into account correctly the transfer of the diffuse continuum (which is not performed in Ballantyne et al. 2001), and that the escape probability approximation gives incorrect results for thick inhomogeneous slabs. Not only this approximation can lead to differences in the line intensities, but also to differences in the energy balance, which is dominated by the line heating/cooling in a large fraction of the illuminated layer. The importance of these processes will be discussed in more detail in a forthcoming paper devoted to this issue (Coupé et al. 2002). Their correct description is clearly an advantage of our model.

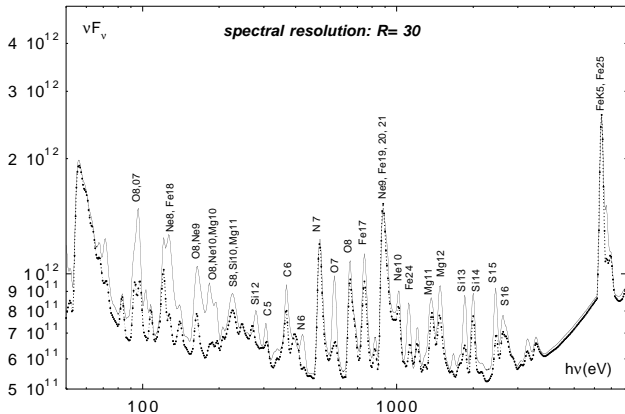


**Figure 16.** Influence of the atomic data on the reflection spectrum for the lamp post model with  $\dot{m} = 0.03$ . Solid line: multi level Li-like, He-like, and H-like ions, dashed line: only multi level H-like ions. Significant difference is only seen below 200 eV.

#### 4.1.2 Atomic data

The importance of heavy elements in illuminated disc atmospheres was clearly shown by Madej & Różańska (2000). Thermal absorption is completely inefficient in pure hydrogen-helium atmospheres, and incident X-ray radiation is redistributed by Comptonization. Iron rich models considered by Madej & Różańska (2000) include only bound-free absorption on iron, but they show completely different spectra with smaller UV bump and a lot of ionization edges which do not exist when Iron is not taken into account.

Obviously the atomic models and atomic data determine directly the line intensities. However they have also an influence on the fractional ionic abundances, through the ionization from, and the recombination onto, the excited states. Indeed close to LTE, i.e. in the dense layers of the atmosphere, ionizations from excited levels almost balance recombinations onto these levels, while in the hot skin, only recombinations onto excited levels are important. Improved atomic data have been recently implemented in the code (cf. Coupé et al. 2002). In particular all Li-like and He-like ions are now treated in a complete interlocked way with 5 to 9 levels plus the continuum, while in the old version of TITAN only H-like atoms were treated with several interlocked excited levels. This is still less than in XSTAR, used by NKK00, but much more than Ballantyne et al. (2001). These new data have been used to compute the spectrum in the lamp post moderate accretion rate case, and they are shown to have an impact on the spectral features in the EUV, but basically not on the vertical disc structure and on the overall continuum spectral distribution (cf. Fig. 16).

#### 4.1.3 Thermal instability issue

Another problem in which one has to choose an approximation is in the approach of the thermal instability.

The vertical structure of the surface irradiated layers of accretion discs is very complex (Różańska & Czerny 1996, hereafter RC96). Illumination of gas in hydrostatic equilibrium by hard X-rays implies the presence of a thermal instability. More precisely, in certain pressure range, the gas can

be in three states of thermal equilibria, with an intermediate one being unstable. The problem is best seen as the presence of S-shape feature in the temperature versus the ionization parameter  $\Xi$  plot (Krolik, McKee & Tarter 1981). There is no unique solutions for the temperature and density profile. Physically, we expect a transition from the upper stable Compton-heated branch to the lower stable branch determined by atomic processes. This transition must happen somewhere in the multi-solution zone and it may be sharp or a two-phase medium may be present.

Unique strict solution of the vertical structure can only be found if electron conduction, in addition to the radiative transfer, is included (Różańska 1999). However, conduction complicates the numerical scheme considerably and at present it was never combined with computations of radiative transfer. In Różańska (1999) radiative transfer was replaced by the energy balance equation, where heating and cooling functions were determined by means of photoionization code CLOUDY appropriate only for moderately thick media (DAC00).

Other papers neglected the conduction term but contained more advanced radiative transfer computations. These papers can be divided into two families, depending on the way of iterating between hydrostatic equilibrium and radiative transfer, which implies their approach to the thermal instability problem.

First family solves strictly both the radiative transfer and hydrostatic equilibrium, iterating density while solving radiative transfer. In this case the problem of appearing multiple solutions is solved by an arbitrary choice of the transition pressure and introducing a discontinuity. This discontinuity, chosen in the first iteration, is preserved in later computations. This approach was taken by Ko & Kallman 1994, and subsequently by Sincell & Krolik (1997, 1999) and Nayakshin, Kazanas & Kallman (2000, hereafter NKK00). The choice of the position of this discontinuity does not influence strongly the resulting spectra (Jimenez-Garate et al. 2001).

Second family keeps the density constant while iterating the temperature at a given computation step. Such a numerical scheme always produces a unique solution across the transition region but at the expense of not providing a strict solution for both radiative transfer and hydrostatic equilibrium in illuminated atmosphere. This approach was used by Raymond (1993), and subsequently by Shimura, Mineshige & Takahara (1995), Madej & Różańska (2000), Kawaguchi, Shimura & Mineshige (2001), and Ballantyne, Ross & Fabian (2001).

Both approaches provide an approximate answer to the problem since the first one does not effectively iterate the optical depth of the hot zone adopted during the first iteration while the second one is never fully converged in the transition zone.

In the present paper we have adopted the second approach. This method gives a solution for the equilibrium temperature which corresponds to an ill defined value of the pressure. The extension of this layer is indicated in Fig. 17 which is an expanded version of Fig. 1, together with the extension of the multiple solution region. We see that the ill-defined region is relatively thin, so one would expect that it has no influence on the overall emitted spectral distribution, but still it may lead to uncertainties in the detailed

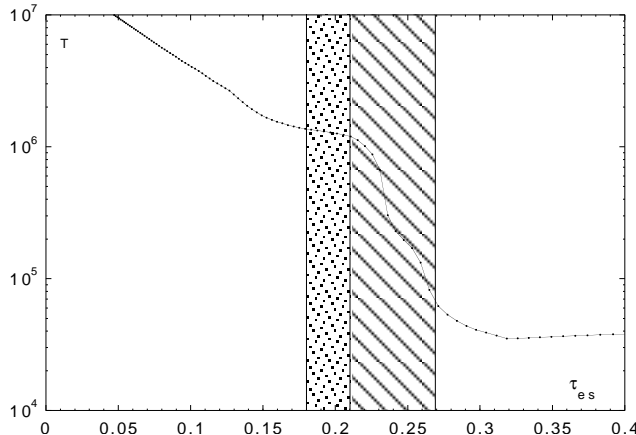


**Figure 17.** The temperature profile for the lamp post model computed with  $\dot{m} = 0.03$ . Grey region: the multiple solution region where the hot solution is chosen; hatched region: ill defined solution (see text).

spectral features, anyway inherent to the presence of the thermal instability; in particular, it contains several important iron ions such as FeXVII. On the other hand the hot solution is suppressed at  $\tau_{es} = 0.21$ , whilst the transition to the cold zone should probably occur at a slightly smaller optical thickness, when conduction is taken into account (cf. below). We have also checked that increasing the number of layers by a factor 2 in the transition zone does not change at all its structure.

#### 4.1.4 Expected effect of conduction

Since our current approach does not include yet the conduction term we test the possible effect of such a term using the local approach of Różańska (1999) and computing the solution for  $\dot{m} = 0.03$  with and without thermal conduction.

Apart from the surface temperature given by the inverse Compton value, one more boundary condition was required to solve the second order differential equation of the energy balance with conduction. This condition was chosen as the requirement that at the bottom of the computed zone the solution matched that of the disc: when the same pressure as in the previous computations was reached, the temperature was also the same.

The dashed line in Fig. 18 represents the temperature profile obtained without radiative transfer but from cooling and heating functions determined from CLOUDY (for better description see RC96). The solid line shows the same computations taking into account thermal conduction. The disc flux, the X-ray flux and the spectral distribution of illuminating radiation are the same as in the lamp post model with  $\dot{m} = 0.03$ .

Clearly, the approach based on local cooling cannot asymptotically reproduce the temperature profile given by the diffusion approximation. The local approach indicates also a certain flattening just below  $10^6$  K which is less important in the TITAN solution. This is due to the lack of the true radiative transfer in this simple exercise.

However we see that in the upper hot zone, the temperature drop occurs faster when thermal conduction is taken

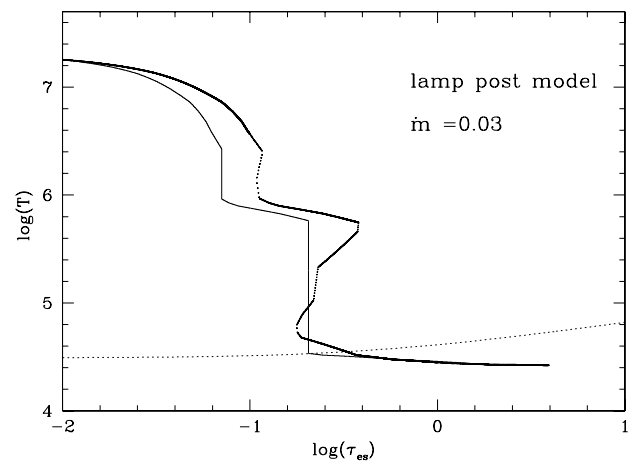


**Figure 18.** The temperature profile for the lamp post model computed with a local approach with (solid line) and without (thick points) thermal conduction. All profiles are computed for the same parameters as the lamp post model with  $\dot{m} = 0.03$ . Dotted line has the same meaning as in Fig. 1.

into account, but finally the total optical depth of the Compton heated zone with thermal conduction is not changed considerably. Therefore, we conclude that the optical depth of the hot layer is determined accurately enough in our radiative transfer calculations without thermal conduction.

#### 4.2 Comparison with other methods

There were many computations of the vertical structure and of the spectrum of irradiated discs for AGN and X-ray binaries in the two past decades. The most recent ones which present spectra including lines from illuminated disc atmosphere with heavy elements in the case of hydrostatic equilibrium are NKK00 and Nayakshin & Kallman (2001), and Ballantyne et al. (2001).

It is extremely difficult to compare directly our results to them, as our computations were performed before the publication of these papers, and therefore adopt other values of the various parameters. For instance the spectral distribution of the incident spectrum is different, a fact of most importance for the structure of the irradiated skin. We have mentioned in the introduction that the spectrum of an irradiated thick layer has been computed using the three codes with exactly the same parameters in the case of a constant density medium (cf. Pequignot et al. 2001). The three computed spectra differ in their overall spectral distribution and in their detailed features. Concerning the model of irradiated disc in hydrostatic equilibrium, for the moment the only possible comparison is to stress the differences between the methods which are used.

Ballantyne et al. results are limited to very high fluxes by their computational method, because their code has difficulty if the hot skin has  $\tau_T \leq 0.2$  (see Sec.6 Ballantyne et al. 2001). It precludes any comparison with their results in the present paper, but this will be achieved in a following paper, dealing with high illumination.

NKK00 use for the thermal and ionization equilibrium the code XSTAR. The advantage is that the atomic physics is better taken into account than by us, but the drawback

is that the total energy balance is not correctly determined (cf. DAC2000 and Coupé et al. 2002). The local energy balance is also not well determined in some cases. In particular, NKK00 were obliged to set the gas temperature equal to the effective one when it was lower. This prevents them to compute the temperature in the deepest irradiated layers. It means that above a given optical thickness, which is of the order of 0.2 in a case comparable to our lamp post models, the temperature becomes constant. This is different from the real temperature structure (cf. Fig. 1). Moreover, they do not compute like us the vertical structure of the underlying disc, but they start their integration from a height given by the Shakura-Sunayev (1973) vertically averaged solution. We show analytically in the appendix that this is valid only if the disc scale height is negligible with respect to the scale height of the irradiated skin, i.e. for low accretion rates ( $< 0.01$  in Eddington units). We have also a completely different way of handling the thermal instability, as NKK00 simply stop their computation when the hot solution disappears, while we compute the structure in the region where the cold solution applies.

The same problems occur in the paper of Ballantyne et al. (2001), where the basis of the hot skin is fixed at the vertically averaged half-thickness of a gas-pressure dominated disc. Also those authors use poor description of heavy elements with only few ionization stages and excited levels. This treatment should underestimate the photoionization heating and the line cooling.

The transfer of the continuum is performed basically in the same way in NKK00 and in our computations, which is better than the approach of Ballantyne et al. who apply the diffusion approximation to the transfer of the diffuse radiation (Ross & Fabian 1993). However both NKK00 and Ballantyne use the Companeets equation for the Compton diffusions, while we take the inelastic scattering into account only above 1 keV, through the coupling of a Monte Carlo code. This is clearly a disadvantage of our method. The transfer of the lines differ also strongly between us and them. Above 1 keV, we use the Monte Carlo code which takes into account Compton diffusion, and below 1 keV, we perform real transfer computation in the lines, but we do not take into account comptonization. So we have the advantage of performing real transfer in the lines, but the disadvantage of not taking into account Compton diffusions. This can have some impact on the intensities of resonance lines which are subject to a large number of scatterings. All other authors use the escape probability formalism for the lines, which however has the advantage to take into account the escape by Compton diffusions.

In their lamp post computations, Nayakshin & Kallman (2001) assume a smaller X-ray flux, with the luminosity of the X-ray source being 20% of the integrated disc luminosity, but nevertheless it corresponds to a larger local flux than ours (they compute the spectrum at  $6R_{Schw}$  and not at  $10R_{Schw}$ ).

NKK00 introduce the “gravity parameter”  $A$  which is the ratio of the vertical component of the gravity force at one disc scale height to the radiation pressure force (for the definition, see NKK00 Sect. 3.3), and they give their results as functions of this parameter. If we calculate the value of parameter  $A$  of NKK00 from our computations of the disc vertical structure we obtain  $A \sim 2$  for both accretion rates.

Indeed this parameter is not sufficient to determine the solution, one must also define the X-ray flux since  $A$  is proportional to the ratio of the viscous to the X-ray flux. So in the following paper, Nayakshin & Kallman (2001) present the NKK00 lamp post models for different accretion rates and X-ray fluxes. Our two models have about the same ratios of viscous to X-ray fluxes and about the same accretion rates as their models w4 and w7. Our models predict an optical depth of the entire hot layer of about 0.2 and 0.4, while in Nayakshin & Kallman the hot layer is almost twice larger. This can be partly due to the spectral distribution of the incident continuum. We adopt a power law with a slope of 0.9 with a cut-off at 100 keV, while their power law has a slope of 0.8 and the continuum curves slowly above 100 keV due to the adopted cut-off. We see clearly that a direct comparison is not possible.

Finally the effect of coronal influence is studied only in case of purely hydrogen atmosphere in the paper of Kawaguchi, Shimura & Mineshige (2001). Since they do not take into account heavy elements, the disc does not absorb X-rays and produces relatively less seed photons for Comptonization. It leads to less efficient coronal cooling and produces rather hard X-ray spectrum even if corona covers the whole disc. This is not the case in our calculations. The disc atmosphere with heavy elements has a low albedo and all absorbed X-ray photons are reemitted in the soft band as seed photons for Comptonization. Therefore, to produce hard X-ray spectrum the corona has to cover the disc only partially.

## 5 CONCLUSIONS

In this paper we have presented computations of the vertical structure and spectrum of an illuminated accretion disc, using a new code available for Compton thick media, TITAN/NOAR, and taking into account hydrostatic equilibrium. The disc atmosphere is integrated vertically together with the disc interior. Below the illuminated atmosphere, for  $\tau_{es} > 6$ , diffusion approximation is used. We compare two geometries: the lamp post model, where an X-ray source is situated above the disc at some distance, and the heavy corona model, where the corona, besides illumination, exerts a dynamical pressure on the disc material. We found:

- In the case of the lamp post model, the uppermost layers of atmosphere are heated to very high temperature which drops suddenly with increasing optical depth. Such a sharp transition is consistent with theoretical predictions and, depending on strength of illumination, may indicate thermal instabilities (KMT81, RC96). The radiative transfer computations prevent the temperature profile to be multivalued, nevertheless thermal instabilities occur as a ‘wiggle’ in the pressure profile. To avoid this problem thermal conduction should be taken into account and we plan to do it in the future work.
- The disc scale height is important for accretion rates  $\dot{m} > 0.01$  (see appendix) and it influences the optical thickness of the illuminated zone. Therefore, it is essential to integrate carefully the cold region below the transition, in order to determine the fractional abundances of weakly ionized heavy elements, which influence the extreme UV and soft X-ray spectrum.

- In case of the lamp post model, the outgoing spectrum differs in extreme UV and soft X-ray band from the case of constant density slab, indicating, that it is extremely important to estimate the temperature and the density in the partially ionized medium. Also  $K_{\alpha}$  iron line looks different in both cases. The absorption edge is absent contrary to the constant density case.
- A heavy corona, even optically thin, completely suppresses the highly ionized zone on the top of the accretion disc.
- The spectrum from the disc covered by a heavy corona is featureless, but it depends on the expected energy distribution of incident radiation. When the X-ray spectrum is hard the energy balance requires that corona covers the disc only partially, and the spectrum from the non covered part becomes important. In such a case it is impossible to distinguish the presence or absence of a patchy corona. When the X-ray spectrum is soft, we can infer the presence of a corona in those objects with featureless spectra.
- Our model is in agreement with recent observations of  $K_{\alpha}$  iron line, where in some objects only the fluorescence component is present (NGC 5548 Yaqoob et al. 2001), in others, only the recombination component is present (Ark 564 Comastri et al. 2001), or like in Mrk 205 (Reeves et al. 2001) both components are seen. It can be explained in the framework of the our model by changing the illuminating X-ray flux.

## APPENDIX A: SEMI-ANALYTICAL RESULTS

A crucial question is how the optical depth of X-ray heated zone depends on explicit calculations of the disc vertical structure.

Let us consider hydrostatic equilibrium with gravity  $g$  and ignoring the term of radiative pressure. We can then simply calculate the optical depth of the hot zone as:

$$\tau_{es}^{hot} = \frac{P_{bot} \kappa_{es}}{g}, \quad (A1)$$

where  $P_{bot}$  is the gas pressure on the bottom of the X-ray heated skin, which can be expressed as:

$$P_{bot} = \frac{F_X}{\Xi_{bot} c}, \quad (A2)$$

The ionization parameter on the bottom,  $\Xi_{bot}$ , is equal to the  $1.22(T_{IC}/10^8)^{-3/2}$  (Begelman, McKee, Shields 1983), with the inverse Compton temperature  $T_{IC}$  defined as usual.

In the case of stellar atmospheres, the optical depth of X-ray heated layer is a function of only the hard X-ray flux and the shape of incident radiation (through the  $T_{IC}$ ):

$$\tau_{es}^{hot} = \frac{F_X \kappa_{es}}{\Xi_{bot} c g}. \quad (A3)$$

In the case of an accretion disc, the gravity depends on the distance from the black hole and on the pressure scale-height of the considered layer (we assume the gravity to be vertically constant). Considering pressure scale-height of the full system i.e. the illuminated zone plus the disc  $H_p = H_{hot} + H_d$ , we can simply derive:

$$\tau_{es}^{hot} = \frac{F_X \kappa_{es}}{\Xi_{bot} c \Omega_K^2} \left( \frac{1}{H_{hot} + H_d} \right), \quad (A4)$$

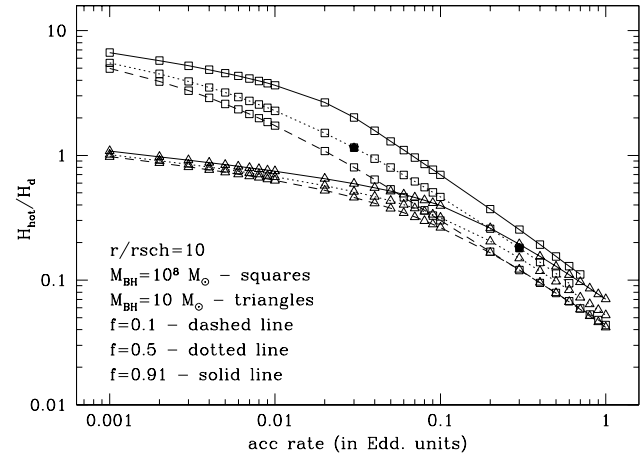


**Figure A1.** The ratio of scale-height of isothermal Compton heated skin to the disc scale-height, versus the accretion rate in Eddington units, for a given radius ( $r = 10R_{Schw}$ ) and for different fractions of energy dissipated in the X-ray source:  $f = 0.1$  - dashed line,  $f = 0.5$  - dotted line, and  $f = 0.91$  - solid line. The results are presented for two different masses of the black hole:  $M_{BH} = 10^8 M_{\odot}$  - squares, and  $M_{BH} = 10 M_{\odot}$  - triangles. Filled squares mark the two cases computed numerically and considered in detail in the previous sections  $\dot{m} = 0.03$  and  $\dot{m} = 0.3$ .

where  $H_{hot}$  is the scale-height of the isothermal Compton heated skin. If  $H_{hot}$  is much larger than  $H_d$  the disc scale-height can be neglected. Rewriting Eq. A4 with Eq. 12 for constant gravity case and replacing  $T_{cor}$  by  $T_{IC}$  one can get:

$$\tau_{es}^{hot} = \frac{F_X \kappa_{es}}{\Xi_{bot} c \Omega_K} \left( \frac{\mu m_H}{k_B T_{IC}} \right)^{1/2}. \quad (A5)$$

For the case of variable gravity the hydrostatic equilibrium should be solved together with the equation of mass continuity  $d\tau = \kappa_{es} \rho dz$ .  $\tau_{es}^{hot}$  is then larger by a factor of  $\sqrt{2}$  (the same factor as for the pressure scale-height, see Eq. 12), and by integral of order of unity (Nayakshin 2000, Eq.2).

If  $H_{hot}$  is comparable to  $H_d$ , the disc structure is important and the optical depth of the X-ray heated skin cannot be determined without proper disc calculations. Fig. A1 gives the ratio  $H_{hot}/H_d$  versus accretion rate for the representative radius  $r = 10R_{Schw}$ .  $H_d$  is computed by solving the explicit disc vertical structure (see Sec. 2.2.1) instead of assuming vertically averaged Shakura & Sunayev disc (1973) like in NKK00. The computations are done for two black hole masses:  $10^8 M_{\odot}$ , which corresponds to the AGN, and  $10 M_{\odot}$ , corresponds to GBHs. We assume different values of  $f$  from low illumination  $f = 0.1$ , which corresponds to  $F_X/F_{disc} = 0.11$ , to strong illumination  $f = 0.91$  which gives  $F_X/F_{disc} = 10$ .

One can see that the ratio is slightly higher for higher  $F_X$  and increases with decreasing accretion rate. Note that in case of GBHs the ratio is always smaller than or equal to unity implying that the disc structure is important for all accretion rates. In case of AGN for  $\dot{m} > 0.04$  the vertical structure of the disc should be integrated down to the midplane to determine correctly the optical depth of the hot skin.

Fig. A2 presents the Thomson thickness of the X-ray heated skin versus the accretion rate for the radius  $10R_{Schw}$  which is expected to be the region where the iron line is

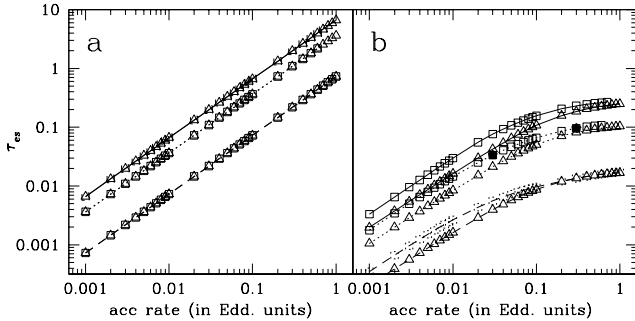


**Figure A2.** The dependence of optical depth of X-ray heated skin on the top of accretion disc on the accretion rate in Eddington units, for the given radius ( $r = 10R_{Schw}$ ) and for different fraction of energy dissipated in the X-ray source:  $f = 0.1$  - dashed line,  $f = 0.5$  - dotted line, and  $f = 0.91$  - solid line. Results are presented for two different masses of the black hole:  $M_{BH} = 10^8 M_\odot$  - squares, and  $M_{BH} = 10 M_\odot$  - triangles. Panel a represents results computed according to Nayakshin (2000) assuming integral equal 1, and panel b is computed for constant gravity Eq. A4 but including the influence of disc structure. Filled squares mark the two solutions computed numerically and considered in the previous sections  $\dot{m} = 0.03$  and  $\dot{m} = 0.3$ .

produced. We compare the analytical results of Nayakshin (2000), who neglect the disc scale-height and shown that this is in agreement with NKK00 numerical computation (see Nayakshin 2000 Fig.1) with ours Eq. A4. One can see that taking into account proper disc calculations it is impossible to obtain optically thick illuminated skin even for the case when  $F_X/F_{disc} = 10$ . Therefore, when observations imply that the hot layer is optically thick, it may be evidence for the existence of hot corona.

## ACKNOWLEDGEMENTS

This work was supported in part by grant 2 P03D 018 16 of the Polish State Committee for Scientific Research and by Jumelage/CNRS No. 16 “Astronomie France/Pologne”.

## REFERENCES

Abrassart A., Czerny, B., 2000, *A&A*, 356, 475  
 Alexander, D.R., Johnson, H.R., Rypma, R.L., 1983, *ApJ*, 272, 773  
 Allen, C.W., 1973, *Astrophysical quantities*. University of London, The Athlone Press  
 Ballantyne, D.R., Ross, R.R., Fabian, A.C., 2001, *MNRAS*, 327, 10  
 Begelman, M.C., McKee, C.F., Shields, G.A., 1983, *ApJ*, 271, 70  
 Branduardi-Raymont, G., Sako, M., Kahn, S. M., Brinkman, A. C., Kaastra, J. S., Page, M. J., 2001, *A&A*, 365, L140  
 Collin, S., Abrassart, A., Czerny, B., Dumont, A.-M., Mouchet, M., 2000, to appear in proc. "AGN in their Cosmic Environment", Eds. B. Rocca-Volmerange & H. Sol, EDPS Conf. Series in Astron. & Astrophysics (astro-ph/0003108)  
 Comastri, A., Stirpe, G.M., Vignali, C., Brandt, W.N., Leighly, K.M., Fiore, F., Guainazzi, M., Matt, G., Nicastro, F., Puchnarewicz, E. M., Siemiginowska, A., 2001, *A&A*, 365, 400  
 Coupé S., et al., 2002, in preparation  
 Czerny B., Zbyszewska M., 1991, *MNRAS*, 249, 634  
 Dumont A.-M., Abrassart A., Collin S., 2000, *A&A*, 357, 823 [DACP00]  
 Dumont A.-M., Collin S., 2001, in "Spectroscopic Challenges of Photonized Plasma", Eds. G. Ferland & D. Savin, ASP Conference Series Vol. XXX  
 Dumont, A.-M., Czerny, B., Collin, S., Mouchet M., Źycki, P., 2001 in preparation  
 Haardt, F., Maraschi, L., 1991, *ApJ*, 380, L51  
 Hubeny, I. 1990, *Structure and Emission Properties of Accretion Discs*, IAU Colloq. 129, 227, Eds Bertout, C., Collin, S., Lasota, J.-P.  
 Jimenez-Garate M.A., Raymond J., Liedahl D.A., Hailey C.J., 2001, *ApJ*, 558, 448  
 Kawaguchi, T., Shimura, T., Mineshige, S., 2001, *ApJ*, 546, 966  
 Ko, Y.-K., Kallman, T.R., 1994, *ApJ*, 431, 273  
 Koratkar, A., Blaes, O., 1999, *PASJ*, 50, 559  
 Krolik, J.H., McKee, C.F., Tarter, C.B., 1981, *ApJ*, 249, 422 [KMT81]  
 Lee, J.C., Ogle, P.M., Canizares, C.R., Marshall, H.L., Schulz N.S., Morales, R., Fabian, A.C., Iwasawa, K., 2001, *astro-ph/0101065*  
 Lightman, A.P., White, T.R., 1988, *ApJ*, 335, 57L  
 Madej, J., Różańska, A. 2000, *A&A* 356, 654  
 Matt, G., Fabian, A.C., Ross, R.R., 1993, *MNRAS*, 264, 839  
 McKee C.F., Begelman M.C., 1990, *ApJ*, 358, 392  
 Nayakshin, S., 2000, *ApJ*, 534, 718  
 Nayakshin, S., Kazanas, D., Kallman, T.R., 2000, *ApJ*, 537, 833  
 Nayakshin, S., Kallman, T.R., 2001, *ApJ*, 546, 406  
 Pequignot D., et al., 2001, in "Spectroscopic Challenges of Photonized Plasma", Eds. G. Ferland & D. Savin, ASP Conference Series Vol. XXX  
 Pojmański, G., 1986, *Acta Astr.*, 36, 69  
 Poutanen J., 1999, in "The Theory of Black Hole Accretion Discs", eds. M.A. Abramowicz, G. Björnson, and J.E. Pringle, Cambridge University Press  
 Raymond, J.C., 1993, *ApJ*, 412, 267  
 Reeves, J.N., Turner, M.J.L., Pounds, K.A., O'Brien, P.T., Boller, Th., Ferrando, P., Kendziorra, E., Vercellone, S., 2001, *A&A*, 365, L134  
 Reynolds, C., 2000, in *Probing the Physics of Active Galactic Nuclei by Multiwavelength Monitoring*, ASP Conference Series, vol. TBD, eds. B.M. Peterson, R.S. Polidan, and R.W. Pogge (astro-ph/0009503)  
 Ross, R.R. 1978, *PhDT*.  
 Ross, R.R., Fabian, A.C., Mineshige, S., 1992, *MNRAS*, 258, 189  
 Ross, R.R., Fabian, A.C., 1993, *MNRAS*, 261, 74  
 Różańska, A. 1999, *MNRAS* 308, 751  
 Różańska, A., Czerny, B., 1996, *Acta Astr.*, 46, 233 [RC96]  
 Różańska A., Czerny B., Źycki P.T., Pojmański G., 1999, *MNRAS*, 305, 481  
 Seaton, M.J., Yan, Y., Mihalas, D., Pradhan, A.K., 1994, *MNRAS*, 266, 805  
 Shakura N.I., Sunyaev R.A. 1973, *A&A*, 24, 337  
 Shimura, T., Mineshige, S., Takahara, F., 1995, *ApJ*, 439, 74  
 Sincell, M.W., Krolik, J.H., 1997, *ApJ*, 476, 605  
 Sincell, M.W., Krolik, J.H., 1998, *ApJ*, 496, 737  
 Suleimanov, V., Meyer, F., Meyer-Hofmeister, E., 1999, *A&A* 350, 63  
 Turner T.J., Romano P. George I.M., Edelson R., Collier S.J., Mathur, S., Peterson, B.M., 2001, *ApJ*, 561, 131  
 Yaqoob, T., George, I. M., Nandra, K., Turner, T. J., Serlemitsos, P. J., Mushotzky, R. F., 2001, *ApJ*, 546, 759  
 Źycki, P.T., Krolik, J.H., Zdziarski, A.A., Kallman, T.R., 1994, *ApJ*, 437, 597

This paper has been processed by the authors using the  
Blackwell Scientific Publications L<sup>A</sup>T<sub>E</sub>X style file.